Application of the Phase Space Quasi-Probability Distribution to the Nuclear Shell Model*

GEORGE A. BAKER, JR.
University of California, Los Alamos Scientific Laboratory, Los Alamos, New Mexico

IAN E. MCCARTHY†
School of Physics, University of Minnesota, Minneapolis, Minnesota, and Department of Physics, University of California, Los Angeles, California

AND

CHARLES E. PORTER‡
School of Physics, University of Minnesota, Minneapolis, Minnesota

(Received April 11, 1960)

The quantum mechanical joint position-momentum quasi-distribution function is applied to the nuclear shell model. By introducing approximate quasi-position and quasi-momentum variables, the quasi-distribution function is converted into a non-negative (and hence nonquasi) distribution. Numerical results are presented for one-dimensional and three-dimensional potentials leading in three dimensions to a nonisotropic nonindependent distribution with a predominance of low momenta at the nuclear surface. These results are in contrast with the usual Thomas-Fermi model and in addition provide a simple base for the discussion of direct nuclear reactions involving an average over many states of a residual nucleus for which linear momentum as opposed to angular momentum is a relevant quantity.

I. INTRODUCTION

INHERENT in the Thomas-Fermi statistical model for a many-body system is the notion of the momentum distribution of one of the typical particles of the system at a given spatial position. From the viewpoint of classical mechanics, the notion of a joint position-momentum probability distribution is not particularly startling; however, from the point of view of quantum mechanics according to which the simultaneous measurements of position and momentum are incompatible, it may seem a little peculiar to discuss such a joint distribution. On the other hand, the use of the position probability distribution $|\psi(q)|^2$, where $\psi(q)$ is the Schrödinger wave function, or the momentum probability distribution $|\varphi(p)|^2$, where $\varphi(p)$ is the momentum wave function, is very familiar.

If we imagine such a joint probability function $f(q,p)$ in one dimension, we would expect at least that

$$|\psi(q)|^2=\int_{-\infty}^{+\infty}dp\, f(q,p), \tag{1}$$

and

$$|\varphi(p)|^2=\int_{-\infty}^{+\infty}dq\, f(q,p). \tag{2}$$

That it is possible to construct a function f which satisfies these two requirements was first shown by Wigner.[1] The function can be written as

$$f(q,p)=\frac{2}{2\pi\hbar}\int_{-\infty}^{+\infty}dy\,\psi^*(q+y)e^{2ipy/\hbar}\psi(q-y), \tag{3}$$

or equivalently

$$f(q,p)=\frac{2}{2\pi\hbar}\int_{-\infty}^{+\infty}dz\,\varphi^*(p+z)e^{2iqz/\hbar}\varphi(p-z). \tag{4}$$

This joint position-momentum quasi-probability distribution function $f(q,p)$ is real, but, in contrast to the corresponding classical distribution function, as an expression of the quantum mechanical incompatibility of the simultaneous complete knowledge of position and momentum, it sometimes takes on negative values, giving it a quasi-probability character.

If we take the Fourier transform of (3) with respect to p, we find

$$\frac{1}{\pi\hbar}\int_{-\infty}^{+\infty}dp\, e^{-2ipw/\hbar}f(q,p)=\frac{2}{2\pi\hbar}\psi^*(q+w)\psi(q-w). \tag{5}$$

Since the variables $q+w$ and $q-w$ are independent, we conclude that despite the "quadratic" appearance of $f(q,p)$, a knowledge of $f(q,p)$ is completely equivalent to a knowledge of $\psi(q)$ [or $\varphi(p)$ by a similar argument]; in fact, it has been shown[2] that the formulation of quantum mechanics can be developed in terms of $f(q,p)$ instead of the more conventional wave functions. In particular, the expected value $\langle O\rangle$ of a measurable quantity $O(q,p)$ is given by

$$\langle O\rangle=\int_{-\infty}^{+\infty}dq\int_{-\infty}^{+\infty}dp\, f(q,p)O(q,p), \tag{6}$$

as would be anticipated for a classical distribution.

All of the above remarks can be carried over to a

* This work supported in part by the U. S. Atomic Energy Commission and the National Science Foundation.

† Permanent address: Department of Mathematical Physics, University of Adelaide, Adelaide, South Australia, Australia.

‡ Present address: Brookhaven National Laboratory, Upton, L. I., New York.

[1] E. P. Wigner, Phys. Rev. **40**, 749(A) (1932).

[2] G. A. Baker, Jr., Phys. Rev. **109**, 2198 (1958). Other pertinent references are given here.

system consisting of n particles with a wave function $\psi(\mathbf{q}_1,\mathbf{q}_2,\cdots,\mathbf{q}_n)$. The n-particle version of (3) is

$$f(\mathbf{q}_1,\mathbf{q}_2,\cdots\mathbf{q}_n,\mathbf{p}_1,\mathbf{p}_2,\cdots,\mathbf{p}_n)$$
$$=\left(\frac{2}{2\pi\hbar}\right)^{3n}\int_{-\infty}^{+\infty}d^3y_1\int_{-\infty}^{+\infty}d^3y_2\cdots\int_{-\infty}^{+\infty}d^3y_n$$
$$\times\psi^*(\mathbf{q}_1+\mathbf{y}_1,\,\mathbf{q}_2+\mathbf{y}_2,\,\cdots,\,\mathbf{q}_n+\mathbf{y}_n)$$
$$\times\exp\left(\frac{2i}{\hbar}\sum_{i=1}^{n}\mathbf{p}_i\cdot\mathbf{q}_i\right)$$
$$\times\psi(\mathbf{q}_1-\mathbf{y}_1,\,\mathbf{q}_2-\mathbf{y}_2,\,\cdots,\,\mathbf{q}_n-\mathbf{y}_n). \quad (7)$$

Again we have the result that the expectation value of a measurable quantity $O(\{\mathbf{q}_i\},\{\mathbf{p}_i\})$ is obtained as

$$\langle O\rangle=\int d^3q_1\int d^3q_2\cdots\int d^3q_n\int d^3p_1\int d^3p_2\cdots\int d^3p_n$$
$$\times f(\{\mathbf{q}_i\},\{\mathbf{p}_i\})O(\{\mathbf{q}_i\},\{\mathbf{p}_i\}). \quad (8)$$

which corresponds as does (6) to the classically anticipated result.

The significance of the quasi-probability distribution for nuclear (or atomic) bound states arises because there are experiments which measure to a good approximation the momentum distribution of bound nucleons (or electrons) in a region of space which is smaller than the whole nucleus (or atom). In general, such an experiment falls into the category of a "direct interaction" experiment in which, to a good approximation, the incident particle interacts with only one nucleon (or electron), and at least for the nuclear case the entrance and exit channel wave functions are so distorted by the remainder of the nucleus, that interactions in some parts of the nucleus are more likely to be observed than those in other parts.

Previously such nuclear experiments have been considered to give information about nuclear momentum distributions. The interaction of high-energy protons (the wave functions of which are only slightly distorted in nuclei) with bound nucleons is found to observe a momentum distribution which approximates that obtained from the momentum transform of bound single-particle wave functions.[3] Anomalously high-momentum components are usually attributed to the effects of strong correlations. The interaction of K^- mesons with a heavy nucleus is well described by assuming that the interactions occur isotropically in the nuclear surface.[4] (Isotropically, here, means no dependence on the angle between the incident direction and the position vector of the collision point.) This assumption of isotropy is also made in the simple direct-interaction theory of Butler[5] and others for low-energy nuclear reactions, but the actual anisotropy of the distribution[6] is known to lead to errors.[7] A low-energy $(p,2p)$ experiment has also been considered to measure the momentum distribution of nucleons localized in an equatorial belt on the nuclear surface.[8] In this case the momentum distribution was assumed to have a Fermi form. The Fermi momentum is practically a meaningless concept since the severe localization leads to a spectrum which may have a completely different shape in the high-momentum region.

II. POSITION-MOMENTUM DISTRIBUTION IN ONE DIMENSION

Before we discuss the joint position-momentum distribution for the nuclear shell model, it is worthwhile to display the character of the quasi-probability function $f(q,p)$ and to show how this quasi-distribution can be related to an actual measurement.

It has already been remarked that the function $f(q,p)$ is everywhere real but not everywhere non-negative. We can remove this non-negative ("quasi-distribution") property by replacing the canonically conjugate variables q and p which cannot be simultaneously sharp by two quasi-variables ξ and η called quasi-position and quasi-momentum, respectively, such that ξ and η can be measured simultaneously and can be interpreted as being very similar to q and p. In general, both ξ and η will depend on *both* q and p *and also the measurement process*, i.e., the coordinates and momenta of the measuring "apparatus." In the case of a $(p,2p)$ reaction, for example, the incident proton and its coupling to the target nucleons (the coupling range determines the amount of localization) make up the measuring "apparatus." It is intended however that ξ be "closely correlated" with q and η with p even though they are not the same dynamical quantities as q and p.

We wish to show that a joint probability distribution (not quasi-probability) for ξ and η exists. This statement is equivalent to saying that the operators representing ξ and η commute. For convenience we will specify a Gaussian correlation function and the variances

$$\langle(\xi-q)^2\rangle=\sigma^2/2,$$
$$\langle(\eta-p)^2\rangle=\hbar^2/2\sigma^2, \quad (9)$$

for which

$$[\langle(\xi-q)^2\rangle\langle(\eta-p)^2\rangle]^{\frac{1}{2}}=\hbar/2, \quad (10)$$

expressing an optimal measurement consistent with the uncertainty principle. We write the joint distribution of ξ and η as [compare to (6)]

[3] K. R. Greider, Phys. Rev. **114**, 786 (1959).
[4] I. E. McCarthy and D. J. Prowse (to be published).
[5] N. Austern, S. T. Butler, and H. McManus, Phys. Rev. **92**, 350 (1953).
[6] I. E. McCarthy, Nuclear Phys. **11**, 574 (1959).
[7] I. E. McCarthy and D. L. Pursey (to be published).
[8] I. E. McCarthy, E. V. Jezak, and A. J. Kromminga, Nuclear Phys. **12**, 274 (1959).

$$b(\xi,\eta;\sigma)=\int_{-\infty}^{+\infty}dq\int_{-\infty}^{+\infty}dp\frac{\exp[-(\xi-q)^2/\sigma^2]}{(\pi\sigma^2)^{\frac{1}{2}}}$$
$$\times\frac{\exp[-\sigma^2(\eta-p)^2/\hbar^2]}{(\pi\hbar^2/\sigma^2)^{\frac{1}{2}}}f(q,p)$$
$$=\frac{2}{2\pi\hbar}\int_{-\infty}^{+\infty}dq\int_{-\infty}^{+\infty}dp$$
$$\times\exp\left(-\frac{(\xi-q)^2}{\sigma^2}-\frac{\sigma^2(\eta-p)^2}{\hbar^2}\right)f(q,p),\quad(11)$$

in which $f(q,p)$ is to be determined from the appropriate wave function according to either (3) or (4). Clearly, since the transformation (11) from $f(q,p)$ to $b(\xi,\eta;\sigma)$ involves difference kernels, it can be readily inverted using Laplace transform techniques so that it is in principle a well-defined process to go from the (non-quasi) probability distribution $b(\xi,\eta;\sigma)$ to the quasi-probability distribution $f(q,p)$ and then to the wave function via (5).

The choice of Gaussian kernels allows us to complete the demonstration that $b(\xi,\eta;\sigma)$ is non-negative. Substituting from (3) into (11) and performing the integration over p by completing the square, we find

$$b(\xi,\eta;\sigma)=\frac{1}{2\pi\hbar}\frac{1}{(\pi\sigma^2)^{\frac{1}{2}}}\int_{-\infty}^{+\infty}dy\int_{-\infty}^{+\infty}dq$$
$$\times\exp\left(-\frac{(\xi-q)^2}{\sigma^2}-\frac{y^2}{\sigma^2}+\frac{2iy\eta}{\hbar}\right)$$
$$\times\psi^*(q+y)\psi(q-y).\quad(12)$$

We now let

$$u=q+y,\qquad v=q-y,\quad(13)$$

for which the transformation Jacobian is $\frac{1}{2}$. This yields for $b(\xi,\eta;\sigma)$

$$b(\xi,\eta;\sigma)=\frac{1}{2\pi\hbar(\pi\sigma^2)^{\frac{1}{2}}}$$
$$\times\left|\int_{-\infty}^{+\infty}\exp\left(-\frac{(\xi-u)^2}{2\sigma^2}-\frac{iu\eta}{\hbar}\right)\psi(u)du\right|^2.\quad(14)$$

Clearly, $b\gtrless 0$ independent of what ψ is assumed. Thus ξ and η are simultaneously measurable,[2] and their joint distribution is given by (14). It is immediately clear from (14) that the quasi-momentum distribution which can in principle be measured locally depends on the size σ of the region of measurement.

It is possible to describe the conventional "snapshot" measurement of ξ and η.[9] The term "snapshot" is

[9] W. Heisenberg, *The Physical Principles of the Quantum Theory* (Dover Publications, Inc., New York, 1930), p. 20 ff.

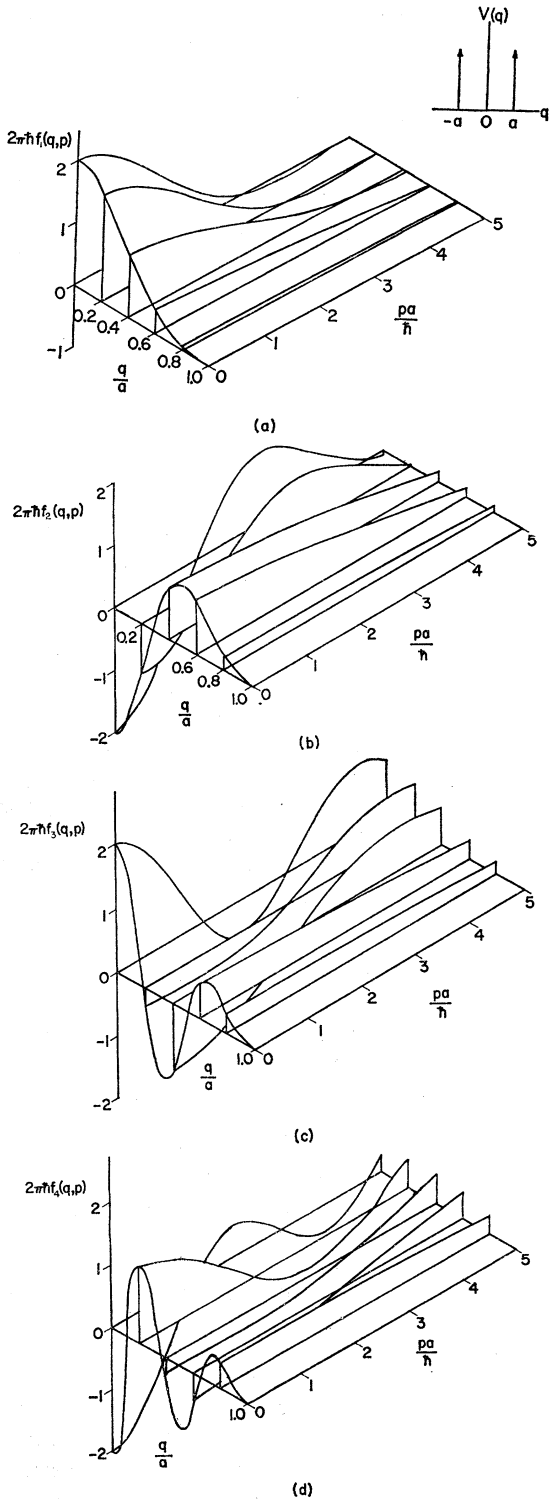

FIG. 1. Plots of the joint position-momentum quasi-probability distribution function $f(q,p)$ as a function of the position q and momentum p for the first four energy levels of a one-dimensional infinite square well of width $2a$. The quantities f, q, and p have been transformed to the dimensionless variables $2\pi\hbar f$, q/a, and $pa/\hbar$. The not-always-positive character of $f(q,p)$ resulting from the uncertainty principle is clearly in evidence.

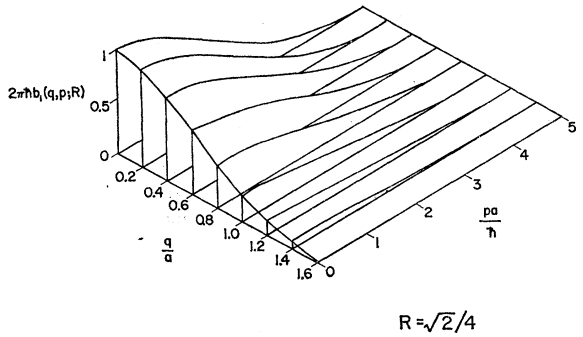

FIG. 2. Plot of the joint probability distribution function $f_1(q,p;R)$ for the first energy level in the one-dimensional infinite square well of Fig. 1 with the resolution constant $R=\sqrt{2}/4$. The variables q and p here are the quasi-position and quasi-momentum variables which are associated with the position and momentum variables of Fig. 1 in the measuring process. The resolution functions describing the measurement of position and momentum are optimal subject to the requirement of measurement consistent with the uncertainty principle. As a result of this consistency, the joint probability distribution function is seen to be always positive. Note that the way in which the measurement is made may yield particles apparently outside the well.

appropriate if we replace the eye of the observer by a photographic film. Two measurements are needed to determine both ξ and η for a particle in motion. To measure ξ with dispersion σ, we use light with wavelength λ such that $\lambda\sim\sigma$. This gives a quasi-position measurement and disperses the momentum. We obtain the quasi-momentum η by taking a second snapshot at a later time with extremely high-frequency light so that in this (the second) measurement the position is precisely known. From the two position measurements and the known time lapse, we calculate an appropriately smeared quasi-momentum η to go with the smeared quasi-position ξ obtained in the first snapshot.

In order to learn about the features of $f(q,p)$ in one dimension, numerical calculations of this function were carried out for the first four states of a one-dimensional infinite square well of width $2a$ centered at $q=0$. The wave function $\psi_n(q)$ appropriate to this problem is

$$\psi_n(q)=\left(\frac{1}{a}\right)^{\frac{1}{2}}\sin\left[\frac{n\pi(q+a)}{2a}\right]. \tag{15}$$

Combining this with (3) we find for the joint quasi-distribution function

$$f_n(q,p)=\frac{n\pi}{2P}\left\{\frac{\sin[(2P-n\pi)(1-|Q|)}{2P-n\pi}-\frac{\sin[(2P+n\pi)(1-|Q|)]}{2P+n\pi}\right\}, \tag{16}$$

$$f_n(0,0)=(-)^{n+1}2,$$

where $Q=q/a$ and $P=pa/\hbar$.

In Fig. 1, plots of $f_n(q,p)$ are shown for the first four states in the well. The regions in which f takes on negative values are very much apparent.

In Figs. 2–7, are shown plots of the joint quasi-position, quasi-momentum distribution function (14) for the potential used in Fig. 1 for various states and for different values of the position resolution $R=\sigma/2a$. To obtain these figures, the wave function of (15) was substituted into (14) and a numerical integration was performed. Beginning with these figures, quasi-position and quasi-momentum are indicated by q and p.

In Fig. 8 the way in which the value of position resolution $R=\sigma/2a$ affects the spreading of the function $b(q,p;\sigma)$ is indicated. This has been done by plotting $b_1(0,0;\sigma)$ as a function of R for the lowest state of the infinite square well.

III. POSITION-MOMENTUM DISTRIBUTION IN THREE DIMENSIONS

In the realistic discussion of the three-dimensional distribution we shall focus our attention on the joint (nonquasi) distribution $b(\mathbf{q},\mathbf{p};\sigma)\equiv b(q,p,x;\sigma)$ where x is the cosine of the angle between $\mathbf{q}$ and $\mathbf{p}$. The three

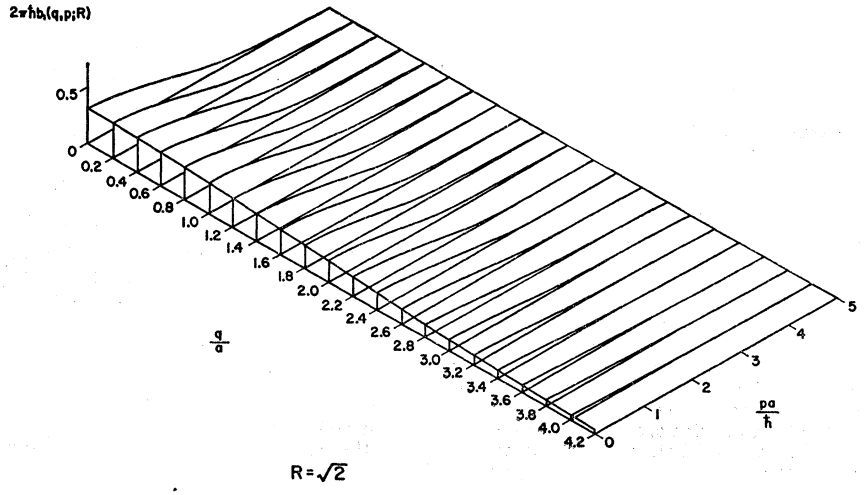

FIG. 3. Plot of the joint probability distribution function of Fig. 2 with $R=\sqrt{2}$. This value of the resolution R tends to smear out the distribution more than that of Fig. 2.

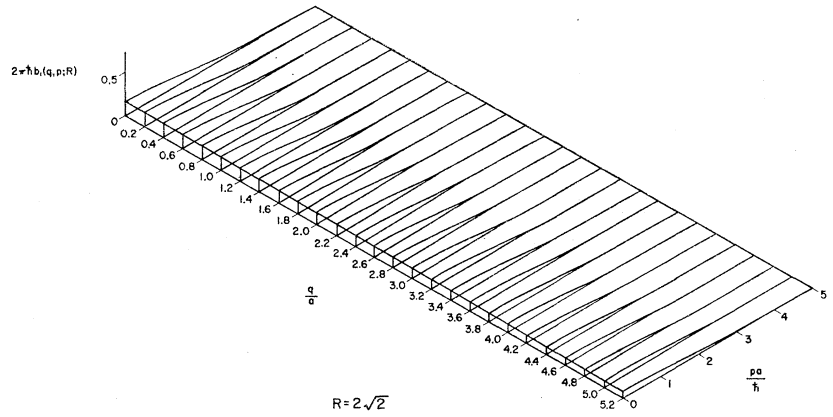

FIG. 4. Plot of the joint probability distribution function of Fig. 2. with $R=2\sqrt{2}$. Even more smearing than shown in Fig. 3 is seen here.

dimensional version of (11) is

$$b(\boldsymbol{\xi},\boldsymbol{\eta};\sigma)=\int\int\int d^3q\int\int\int d^3p\frac{\exp[-(\boldsymbol{\xi}-\mathbf{q})^2/\sigma^2]}{(\pi\sigma^2)^{\frac{3}{2}}}\times\frac{\exp[-\sigma^2(\boldsymbol{\eta}-\mathbf{p})^2/\hbar^2]}{(\pi\hbar^2/\sigma^2)^{\frac{3}{2}}}f(\mathbf{q},\mathbf{p}). \quad (17)$$

By following procedures directly analogous to those leading to (14), we replace (14) by

$$b(\mathbf{q},\mathbf{p};\sigma)=\frac{1}{(2\pi\hbar)^3}\frac{1}{(\pi\sigma^2)^{\frac{3}{2}}}\times\left|\int\int\int d^3u\exp\left(-\frac{(\mathbf{q}-\mathbf{u})^2}{2\sigma^2}-\frac{i\mathbf{u}\cdot\mathbf{p}}{\hbar}\right)\psi(\mathbf{u})\right|^2, \quad (18)$$

where now $\mathbf{q}$ and $\mathbf{p}$ replace $\boldsymbol{\xi}$ and $\boldsymbol{\eta}$ as the quasi-variables and $\psi(\mathbf{u})$ is the appropriate three-dimensional wave function.

We wish to examine the distribution $b(q,p,x;\sigma)$ for the nuclear shell model. Thus we consider a single particle state ψ_{nljm} specified by the quantum numbers $nljm$. In general, we will not distinguish between states

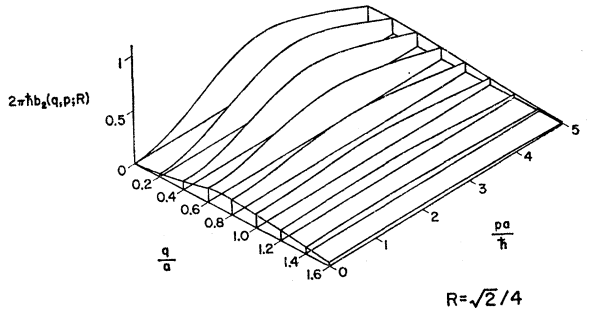

FIG. 5. Plot of the joint probability distribution function $b_2(q,p;R)$ for the second energy level of the infinite one-dimensional square well of Fig. 1 with the resolution constant $R=\sqrt{2}/4$ as a function of the quasi-variables q and p. The beginning of additional spatial structure is seen here as well as the shift of the momentum peak to $pa/\hbar\simeq 2(\pi/2)=\pi$.

with different m values so that we construct the function $b_{nlj}(q,p,x;\sigma)$ which represents an average of the distribution over m values:

$$b_{nlj}(q,p,x;\sigma)=\frac{1}{2j+1}\sum_{m=-j}^{j}b_{nljm}(q,p,x;\sigma). \quad (19)$$

This becomes, upon using (18)

$$b_{nlj}(q,p,x;\sigma)=\frac{1}{(2\pi\hbar)^3}\frac{1}{(\pi\sigma^2)^{\frac{3}{2}}}\frac{1}{2j+1}\sum_{m=-j}^{+j}|I_{nljm}'|^2, \quad (20)$$

where

$$I_{nljm}'(q,p,x;\sigma)=\int\int\int d^3u\times\exp\left(-\frac{(\mathbf{q}-\mathbf{u})^2}{2\sigma^2}-\frac{i\mathbf{u}\cdot\mathbf{p}}{\hbar}\right)\psi_{nljm}(\mathbf{u}). \quad (21)$$

It is convenient to introduce the dimensionless variables

$$\mathbf{U}=\mathbf{u}/\sigma,\quad \mathbf{Q}=\mathbf{q}/\sigma,\quad \mathbf{P}=\mathbf{p}\sigma/\hbar, \quad (22)$$

and the expression

$$I_{nljm}(q,p,x;\sigma)=\int_0^\infty dU\,U^2\int d\Omega_U\exp[-\tfrac{1}{2}U^2-i(\mathbf{P}+i\mathbf{Q})\cdot\mathbf{U}]\times R_{nlj}(U\sigma)Y_{jm}(\Omega_U), \quad (23)$$

so that

$$I_{nljm}'=\sigma^3\exp(-\tfrac{1}{2}Q^2)I_{nljm}, \quad (24)$$

where R_{nlj} is the single particle radial wave function and $\mathcal{Y}_{jm}$ is the appropriate angular momentum function. In the case of no spin, $j=l$ and $\mathcal{Y}_{jm}=Y_{lm}(\Omega_U)$ where Y_{lm} is a spherical harmonic. We then have

$$I_{nlm}=\int_0^\infty dU\,U^2\exp(-\tfrac{1}{2}U^2)R_{nl}(U\sigma)\times\int d\Omega_U\exp[-i\mathbf{U}\cdot(\mathbf{P}+i\mathbf{Q})]Y_{lm}(\Omega_U). \quad (25)$$

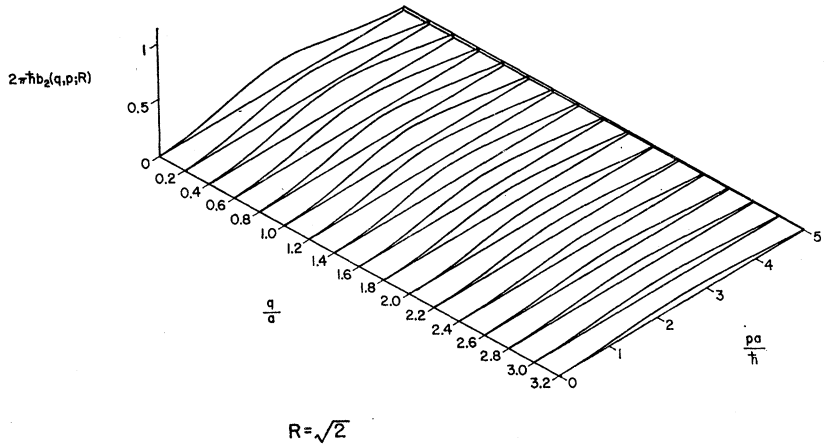

FIG. 6. Plot of the joint probability distribution function $b_2(q,p;R)$ as in Fig. 5 for $R=\sqrt{2}$. This choice of resolution clearly smears out the distribution.

This leads us to introduce the complex vector $\boldsymbol{\zeta}$ such that

$$\begin{aligned}&\boldsymbol{\zeta}=-(\mathbf{P}+i\mathbf{Q}),\\&\zeta^2=\boldsymbol{\zeta}\cdot\boldsymbol{\zeta}=P^2-Q^2+2iPQx,\\&x=\mathbf{P}\cdot\mathbf{Q}/PQ.\end{aligned}\tag{26}$$

In addition we define

$$f_{nl}(U)=U^2\exp(-\tfrac{1}{2}U^2)R_{nl}(U\sigma).\tag{27}$$

Hence the angular integration becomes

$$\begin{aligned}&\int d\Omega_U\exp(i\mathbf{U}\cdot\boldsymbol{\zeta})Y_{lm}(\Omega_U)\\&\quad=4\pi\int d\Omega_U\sum_{l'm'}i^{l'}j_{l'}(U\zeta)Y_{l'm'}{}^*(\Omega_U)\\&\qquad\times Y_{l'm'}(\Omega_\zeta)Y_{lm}(\Omega_U).\end{aligned}\tag{28}$$

By using the orthogonality of the spherical harmonics we find

$$I_{nlm}=\int_0^\infty dU\,f_{nl}(U)i^lj_l(U\zeta)Y_{lm}(\Omega_\zeta).\tag{29}$$

(Although $d\Omega_\zeta$ is a complex solid angle, the addition formulas usually stated for spherical harmonics still hold.) Carrying out the average over m yields

$$\begin{aligned}&\frac{1}{2l+1}\sum_{m=-l}^{m=+l}|I_{nlm}|^2\\&\quad=\frac{16\pi^2}{2l+1}\left|\int_0^\infty dU\,f_{nl}(U)j_l(U\zeta)\right|^2\\&\qquad\times\sum_{m=-l}^{+l}Y_{lm}{}^*(\Omega_{\zeta^*})Y_{lm}(\Omega_\zeta),\\&\quad=4\pi\left|\int_0^\infty dU\,f_{nl}(U)j_l(U\zeta)\right|^2P_l\left(\frac{\boldsymbol{\zeta}^*\cdot\boldsymbol{\zeta}}{|\zeta|^2}\right).\end{aligned}\tag{30}$$

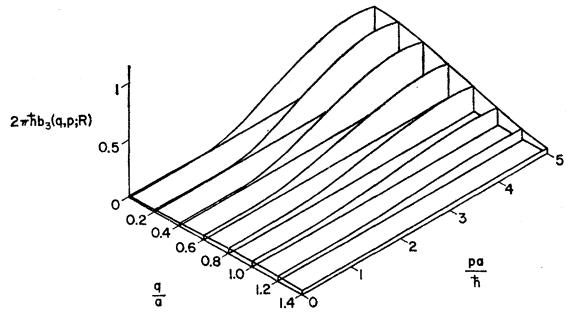

FIG. 7. Plot of the joint probability distribution function $b_3(q,p;R)$ for the third energy level in an infinite one-dimensional square well with resolution constant $R=\sqrt{2}/4$ as a function of quasi-position q and quasi-momentum p. The movement of the major momentum peak to $pa/\hbar\simeq 3(\pi/2)$ is clearly shown.

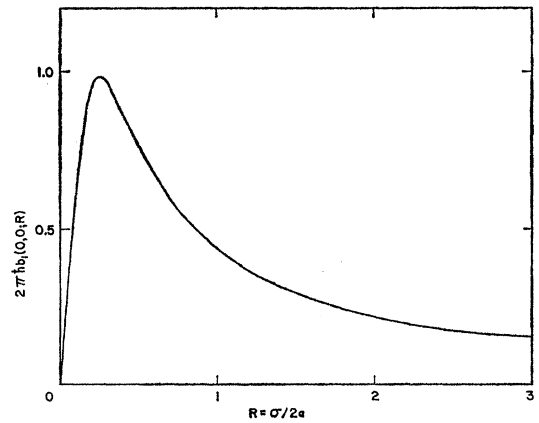

FIG. 8. Plot of the joint probability distribution function $b_1(0,0;R)$ for the first energy level in the infinite one-dimensional square well evaluated at quasi-position $q=0$ and quasi-momentum $p=0$ as a function of the resolution parameter $R=\sigma/2a$ where $2a$ is the width of the well as in Fig. 1. The optimum value of R is seen to be $R\simeq\frac{1}{4}$. Since the function $b_1(q,p;R)$ is monotonically decreasing in q and p, this plot gives a fairly accurate idea of the resolution dependence for a large q-p region.

Combining our results we find in the case of no spin

$$b_{nl}(Q,P,x;\sigma) = \frac{\sigma^3}{(2\pi\hbar)^3}\frac{4}{\pi^{\frac{1}{2}}}\exp(-Q^2) \times\left|\int_0^\infty dU\, U^2\exp(-\tfrac{1}{2}U^2)R_{nl}(U\sigma)j_l(U\zeta)\right|^2 \times P_l\left(\frac{\zeta^*\cdot\zeta}{|\zeta^2|}\right), \quad (31)$$

in which

$$\zeta=(\zeta\cdot\zeta)^{\frac{1}{2}}=(P^2-Q^2+2iPQx)^{\frac{1}{2}},$$
$$\frac{\zeta^*\cdot\zeta}{|\zeta^2|}=\frac{P^2+Q^2}{[\,|P^4+Q^4-2P^2Q^2(1-2x^2)|\,]^{\frac{1}{2}}}. \quad (32)$$

In the case of spin-orbit splitting, the result is identical to (31) provided the label nl is replaced by nlj:

$$b_{nlj}(Q,P,x;\sigma) = \frac{\sigma^3}{(2\pi\hbar)^3}\frac{4}{\pi^{\frac{1}{2}}}\exp(-Q^2) \times\left|\int_0^\infty dU\, U^2\exp(-\tfrac{1}{2}U^2)R_{nlj}(U\sigma)j_l(U\zeta)\right|^2 \times P_l(\zeta^*\cdot\zeta/|\zeta^2|), \quad (33)$$
$$\equiv b_s(Q,P,x;\sigma),$$

where s denotes a shell model state. As we remarked concerning the one-dimensional distribution, it is possible in principle using three-dimensional Fourier transforms to unravel the quasi-distribution f from the distribution b and then to proceed from f to the wave function.

Under the circumstance $x=0$ (tangential momentum distribution), special treatment of (32) or (33) is needed for $P\to Q$. By using the formulas for the spherical Bessel function $j_l(U\zeta)$ for small argument (since $\zeta\to 0$) and the asymptotic formulas for the Legendre function $P_l(\zeta^*\cdot\zeta/|\zeta^2|)$ for large argument, it is possible to show, for example, that (33) becomes

$$b_s(Q,P,0;\sigma)\underset{P\to Q}{\longrightarrow}\frac{\sigma^3}{(2\pi\hbar)^3}\frac{4}{\pi^{\frac{1}{2}}}\exp(-Q^2) \times\left|\int_0^\infty dU\, U^{l+2}\exp(-\tfrac{1}{2}U^2)R_{nlj}(U\sigma)\right|^2 \times\frac{\pi^{\frac{1}{2}}}{(2l+1)^2\Gamma(l+\frac{1}{2})\Gamma(l+1)}Q^{2l}, \quad (34)$$

in which $\Gamma(z)$ is the standard gamma function.

The functions $b_s(q,p,x;\sigma)$ have been computed for all of the neutron wave functions for carbon. The wave functions that were used were obtained for an Eckart potential[10] using the parameters of Ross, Mark, and Lawson.[11] This potential is

$$V(q)=-V_0/(1+e^{(q-R)/a}), \quad (35)$$

with

$$R=r_0A^{\frac{1}{3}},\quad r_0=1.3\times10^{-13}\text{ cm},$$
$$V_0=42.8\text{ Mev}, \quad (36)$$
$$a=0.69\times10^{-13}\text{ cm},$$

in which A signifies atomic weight.

In Fig. 9 plots are made of b_s summed over the neutron states and averaged over the angle between **q** and **p**, i.e., of

$$(2\pi\hbar)^3\sum_s\tfrac{1}{2}\int_{-1}^{+1}dx\, b_s(q,p,x;\sigma). \quad (37)$$

The curves for each value of σ have been arbitrarily

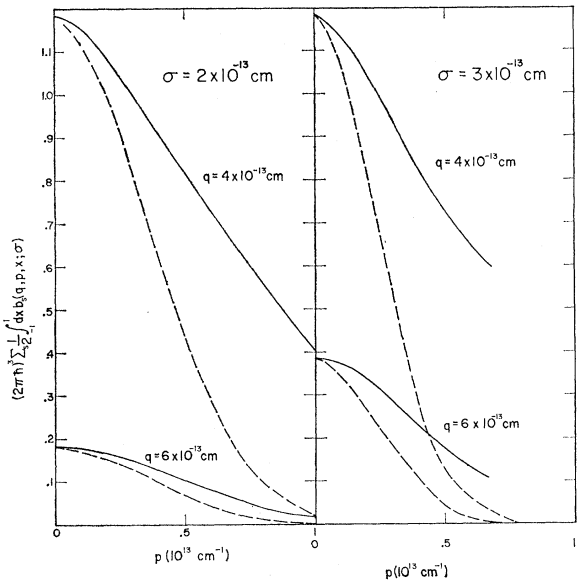

FIG. 9. Plots of the three-dimensional joint probability distribution function for carbon summed over the $1s$ and $2p$ states and averaged over the cosine of the angle between the vectors **q** and **p**. These calculations are based on wave functions obtained from an Eckart potential (reference 11) with a radius parameter of 2.98×10^{-13} cm, a surface diffuseness parameter of 0.69×10^{-13} cm, and a depth of 42.8 Mev. Two different values of the resolution width σ are shown with plots (arbitrarily normalized for each σ value) being made versus quasi-momentum for two different quasi-positions q in the nucleus. The dashed curves show the shapes (arbitrarily normalized to the solid curves at $p=0$) of the momentum resolution functions corresponding to the space resolution width σ. The purpose of this plot is to show that additional information beyond the shape of the resolution function can be obtained, and to indicate that low-momentum values are found near the edge of the nucleus.

[10] C. Eckart, Phys. Rev. **35**, 1303 (1930).

[11] A. A. Ross, H. Mark, and R. D. Lawson, Phys. Rev. **102**, 1617 (1956).

normalized so that the left-hand scale has only relative meaning within each σ set. Dashed curves representing arbitrarily normalized Gaussian momentum resolution functions with width $\hbar^2/2\sigma^2$ [see (9)] are also shown to emphasize that more than just the shape of the resolution function emerges from the computations. Since the radius of carbon used here is 2.98×10^{-13} cm and the spatial resolution is $2\text{–}3\times10^{-13}$ cm, the positions chosen in Fig. 9 are "in the edge" ($q=4\times10^{-13}$ cm) or "out in the tail" ($q=6\times10^{-13}$ cm) of the potential, respectively. The computations clearly indicate a preference for low momentum values in this region.

In Fig. 10 a plot has been made of the ratio of the two solid curves with $\sigma=2\times10^{-13}$ cm from Fig. 9. It might be thought (in the spirit of the Thomas-Fermi model) that the resulting distribution plotted in Fig. 9 would be composed of two independent distributions of q and p separately. Fig. 10 provides a counter-example, i.e.,

$$(2\pi\hbar)^3\sum_s \tfrac{1}{2}\int_{-1}^{+1} dx\, b_s(q,p,x;\sigma)\neq\alpha(q)\beta(p). \qquad (38)$$

It is also possible to ask if the distribution functions depend in a significant way on the rounding of the edge of the well. To answer this question computations were carried out for a square well very similar to that of Levinson and Banerjee.[12] The potential well used was

$$\begin{aligned} V(q)&=-V_0,\ q\leqslant R,\\ V(q)&=0,\ q>R \end{aligned} \qquad (39)$$

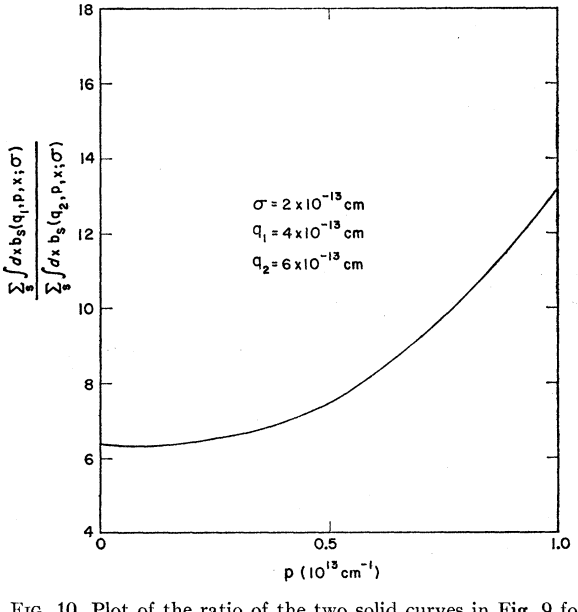

FIG. 10. Plot of the ratio of the two solid curves in Fig. 9 for $\sigma=2\times10^{-13}$ cm against quasi-momentum. This plot demonstrates that even after angular averaging the quasi-position q and quasi-momentum p are not independently distributed; for independent distributions (e.g., the Thomas-Fermi model) the ratio would be constant for all quasi-momentum values.

[12] C. A. Levinson and M. K. Banerjee, Ann. Phys. 3, 67 (1958).

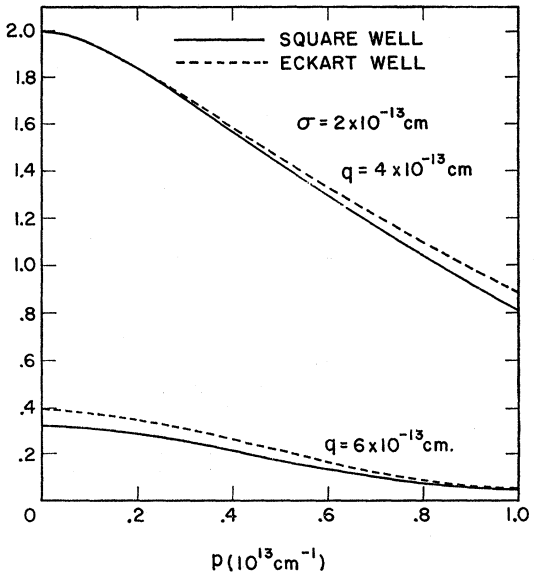

FIG. 11. Comparison of square well calculations with Eckart (rounded) well calculations for the $1p$ state of carbon. The square well (radius 3.66×10^{-13} cm and depth 28.7 Mev) is very close to that used by Levinson and Banerjee (reference 12) in an inelastic scattering calculation. The Eckart well represents a choice based on best fits to energy levels over the periodic table according to Ross, Mark, and Lawson (reference 11) and is the same as used in Fig. 9. The $q=4\times10^{-13}$ cm. Curves for each well are arbitrarily normalized to the same number on the vertical scale. This plot indicates that only a small effect in the momentum distribution results from very different potentials.

with

$$\begin{aligned} V_0&=28.7\text{ Mev},\\ R&=3.66\times10^{-13}\text{ cm}. \end{aligned} \qquad (40)$$

There is no spin-orbit term. The results shown in Fig. 11 are for the $1p$ state of carbon together with the rounded well (Eckart) which is the same as that used in Fig. 9. Although the potentials used are quite different, very little change is seen to occur in the distribution. It is tempting to infer from this plot (although an actual calculation should be made as a check) that using a distorted (nonspherical) potential would not produce very significant changes in the distribution. However, there is the more likely possibility that the angular dependence of the distribution which has been averaged out here might be changed in an important way by distorting the potential.

Beginning with Fig. 12, we examine the angular features of the distribution $b(q,p,x;\sigma)$. It is particularly convenient to define the radial and tangential components of the vector $\mathbf{p}$:

$$\begin{aligned} \mathbf{p}_r&=(\mathbf{p}\cdot\mathbf{q})\mathbf{q}/q^2,\\ \mathbf{p}_t&=\mathbf{p}-\mathbf{p}_r\\ &=\mathbf{q}\times(\mathbf{p}\times\mathbf{q})/q^2. \end{aligned} \qquad (41)$$

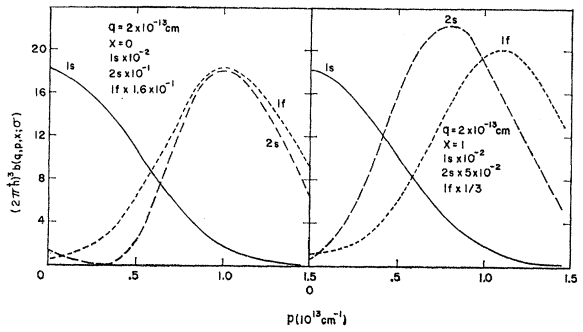

FIG. 12. Plots of the tangential ($x=0$) and radial ($x=1$) quasi-momentum distributions for the $1s$, $2s$, and $1f$ states in Ca^{40} with the quasi-position $q=2\times10^{-13}$ cm and the resolution width $\sigma=2\times10^{-13}$ cm. The parameters used here for the Eckart well (reference 11) are a radius of 4.44×10^{-13} cm and edge diffuseness of 0.69×10^{-13} cm, well depth of 42.8 Mev, and a spin-orbit parameter λ of 39.5. Scaling factors for the various curves are indicated on the plot.

In terms of the variable x, these are

$$\mathbf{p}_r=x\mathbf{p}\mathbf{q}/q,$$
$$\mathbf{p}_t=(1-x^2)^{\frac{1}{2}}p\frac{\mathbf{q}\times(\mathbf{p}\times\mathbf{q})}{|\mathbf{q}\times(\mathbf{p}\times\mathbf{q})|}. \tag{42}$$

Clearly

$$p^2=p_r^2+p_t^2,$$
$$\mathbf{p}=\mathbf{p}_r+\mathbf{p}_t. \tag{43}$$

We are particularly interested in the angular momentum $\mathbf{L}$ of the particle; this is

$$\mathbf{L}=\mathbf{q}\times\mathbf{p}=\mathbf{q}\times\mathbf{p}_t, \tag{44}$$

since $\mathbf{q}\times\mathbf{p}_r=0$. But we can write

$$\mathbf{p}_t=\mathbf{q}\times(\mathbf{p}\times\mathbf{q})/q^2=(\mathbf{q}\times\mathbf{p})\times\mathbf{q}/q^2,$$
$$=\mathbf{L}\times\mathbf{q}/q^2, \tag{45}$$

or

$$p_t^2=(\mathbf{L}\times\mathbf{q})\cdot(\mathbf{L}\times\mathbf{q})/q^4,$$
$$=L^2/q^2, \tag{46}$$

since $\mathbf{q}\cdot\mathbf{L}=0$.

The energy of a particle in a potential $V(q)$ is

$$E=p^2/2M+V(q),$$
$$=p_r^2/2M+p_t^2/2M+V(q),$$
$$=p_r^2/2M+L^2/2Mq^2+V(q), \tag{47}$$

For a state of definite orbital angular momentum, $L^2=\hbar^2l(l+1)$, so that

$$\frac{p_r^2}{2M}=E-V(q)-\frac{\hbar^2l(l+1)}{2Mq^2}. \tag{48}$$

This equation enables us to get an idea of the expected value of p_r at some radial position q. The expected value of p_t is given by (46).

We can obtain typical estimates of p_t and p_r for a nucleon by considering $E=-8$ Mev, $V(q)=-40$ Mev, $q=3\times10^{-13}$ cm, and $l=1$. This gives

$$p_r\simeq1.08\times10^{13}\text{ cm}^{-1},$$
$$p_t\simeq0.33\times10^{13}\text{ cm}^{-1}. \tag{49}$$

Note that $p_r\gg p_t$; for low angular momentum states, this is a typical result. Thus a very nonisotropic local behavior for the momentum distribution is clearly indicated in regions of strong potential, and this feature is born out by the numerical computations.

Figures 12–14 show the results of numerical calculations of the tangential ($x=0$) and radial ($x=1$) quasi-momentum distributions for three states of Ca^{40}. Each figure corresponds to a different radial position. The potential that was used for these calculations is the same as (35) with an added "derivative type" of spin-orbit term.[11]

$$V(q)=\frac{-V_0}{1+\exp[(q-R)/a]}$$
$$-\lambda\left(\frac{\hbar}{2Mc}\right)^2\frac{V_0\exp[(q-R)/a]}{a\{1+\exp[(q-R)/a]\}^2}\frac{2\mathbf{L}\cdot\mathbf{S}}{\hbar^2}, \tag{50}$$

where

$$\frac{2\mathbf{L}\cdot\mathbf{S}}{\hbar^2}=\begin{cases}l, & j=l+\frac{1}{2},\\ -(l+1), & j=l-\frac{1}{2}.\end{cases} \tag{51}$$

The numerical values of the parameters that were used in the machine computations are

$$R=r_0A^{\frac{1}{3}},\quad r_0=1.3\times10^{-13}\text{ cm},$$
$$V_0=42.8\text{ Mev},$$
$$a=0.69\times10^{-13}\text{ cm},$$
$$\lambda=39.5. \tag{52}$$

These parameters are identical to those of (36) except that $A=40$ for calcium and $\lambda\neq0$.

A study of Figs. 12–14 indicates the relative predominance of low quasi-momentum components near the surface of the nucleus compared to the behavior of the momentum distribution inside of the nucleus (the radius of calcium used here is 4.45×10^{-13} cm). In addition the favoring of large radial quasi-momentum components compared to tangential components is

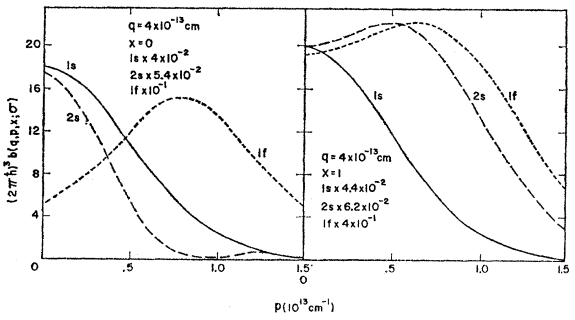

FIG. 13. Plots of the same functions shown in Fig. 12 for quasi-position $q=4\times10^{-13}$ cm.

evident in Figs. 13 and 14. The large amount of tangential quasi-momentum associated with the $2s$ state at $q=2\times10^{-13}$ cm may be from uncertainty in direction for such small q values.

In Fig. 15, the definite non-isotropic character of the distribution is indicated by fixing the magnitudes of **q** and **p** and plotting the distribution against x, the cosine of the angle between **q** and **p**. This plot contrasts with the usual viewpoint of the Thomas-Fermi model which would predict an isotropic result.

IV. COMMENTS AND CONCLUSIONS

The usual direct interaction theories[5] for reactions leading to low excited states of a residual nucleus place overwhelming emphasis on the importance of the angular momentum transfer involved in the reaction. At first sight, this may seem to be in conflict with the viewpoint (emphasizing linear momentum) of this paper. The reconciliation of these two points of view is achieved by noting that the arguments presented here are not to be applied to reactions leading to a single final state (with well-defined angular momentum) of the residual nucleus; only when the reaction measurement averages over many final states can the notion of linear momentum come into play since a state of well-defined angular momentum is a superposition of many states of well-defined linear momentum and vice-versa. One immediate consequence of these statements is that it might be rather suggestive to examine joint quasi-angular-momentum and quasi-angle distributions to see what insights can be obtained into the usual direct interaction theories.

The large effect of the localization of a reaction on the measured momentum distribution may explain the inability of plane wave direct interaction theory to account for the fact that a diffraction pattern is generally not observed in nuclear inelastic scattering when the particles are sharply focused by the optical potential. A simple JWKB calculation[13] which does not take into account localization, predicts that the diffraction "wiggles" in sharply focused nuclear inelastic scattering should be more pronounced than for strongly absorbed alpha particles for which the focus is not significant. This is opposite to the experimental facts. Where a restricted part of the nucleus is sampled, the momentum spread largely eliminates the diffraction pattern arising from the interference of exit channel waves coming from opposite sides of the nucleus and characterized by a length of the order of the nuclear radius. This concept will be developed in a future publication.[7]

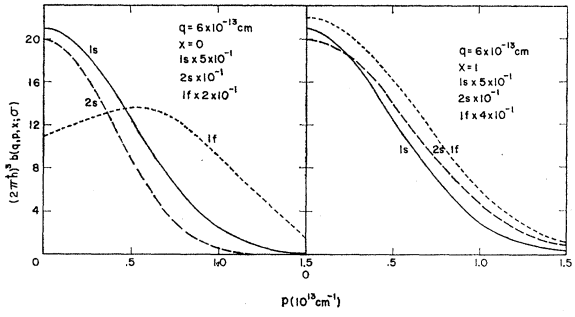

FIG. 14. Plots of the same functions shown in Fig. 12 for quasi-position $q=6\times10^{-13}$ cm. Comparison of this plot to those of Figs. 12 and 13 shows the relative predominance of lower quasi-momentum values at the surface of the nucleus. Both Figs. 13 and 14 indicate a mean radial quasi-momentum larger than the mean tangential quasi-momentum.

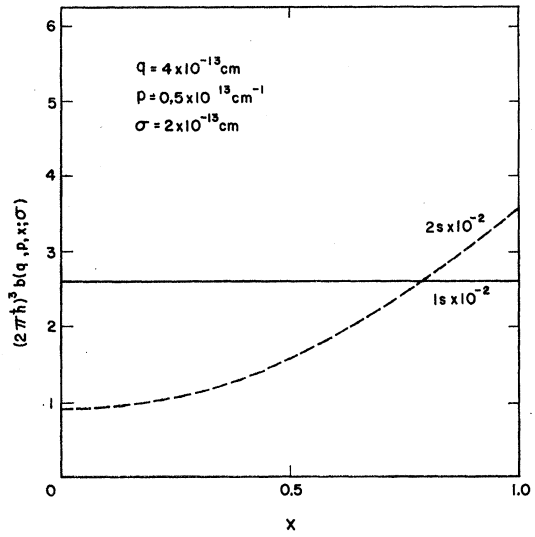

FIG. 15. Plot of the angular variations (x is the cosine of the angle between q and p) of the probability distributions for fixed values of σ, q, and p: $\sigma=2\times10^{-13}$ cm, $q=4\times10^{-13}$ cm, $p=0.5\times10^{+13}$ cm^{-1}. Scaling factors for the curves are indicated on the plot which is based on the wave functions used in Fig. 13. The definite nonisotropic character of this dependence is in contrast to the Thomas-Fermi model. The distribution is symmetric about $x=0$, i.e., about the angle between **q** and **p** equal to 90°.

The sharp differences between the joint distribution considered in this paper and the Thomas-Fermi model have been pointed out: the directionally averaged joint distribution is not a composite of independent distributions of quasi-position and quasi-momentum, and the unaveraged distribution is not isotropic. In addition, the prevalence of low quasi-momenta at the nuclear surface has been emphasized as well as the predominance of the radial over the tangential quasi-momentum there. These features result in a simple picture of, for example, a $(p,2p)$ reaction.[14,15] The reaction is viewed as a "chipping" reaction occurring primarily in an equatorial belt of the target nucleus located in a plane perpendicular to the direction of the incident beam.

[13] S. T. Butler, N. Austern, and C. Pearson, Phys. Rev. **112**, 1227 (1958).

[14] R. J. Griffiths and R. M. Eisberg, Nuclear Phys. **12**, 225 (1959); T. J. Gooding and H. G. Pugh, Nuclear Phys. (to be published).

[15] A. J. Kromminga and I. E. McCarthy, Phys. Rev. Letters **4**, 288 (1960).

The main momentum component (radial) of a nucleon in the target nucleus in this equatorial belt is perpendicular to the momentum of the incident particle. Arguments for a 90° collision between two unbound particles would lead to a final sharp angular correlation between them centered at 90°; however, the non-zero binding energy of the nucleon in the target shifts this to an angular correlation centered near 60° in closer accord with experiment. The actual formula for the angle θ between the two final protons is

$$\cos\theta = |V|/2(E_{1f}E_{2f})^{\frac{1}{2}}, \tag{53}$$

where E_{1f} and E_{2f} are the final kinetic energies of the two protons and V is the strength of the potential binding the bound proton at the point of collision. The sharp character of the angular correlation peak is accounted for by the small tangential (as compared to radial) momentum component since only this component broadens the peak. In addition, the momentum distribution corresponding to the bound nucleon favors low momenta and has a shape more characteristic of the localization than of the structure of the wave function of the bound nucleon.

It is, of course, very tempting to consider the application of the techniques discussed here to atomic and molecular reaction problems. The extent to which a screened Coulomb potential may alter the preceding discussion is presently not well understood.

The formalism discussed here is clearly generalizable to a joint distribution for more than one particle as indicated in (7). Generalizations of this sort could prove useful for discussing reactions involving composite systems.

ACKNOWLEDGMENTS

The numerical computations reported in this paper were carried out using IBM-709 computers at the Northern States Power Company in Minneapolis and at the University of California in Los Angeles. We would like to thank C. E. Giebler and A. G. Montgomery of the Northern States Power Company for making the machine time available to us and for advice and assistance pertinent to coding problems. Similarly at UCLA we have benefited from the help of Dr. M. A. Melkanoff and D. Cantor with regard to coding problems; our thanks are due them also for providing the bound state wave functions used in these calculations.

We would like to thank E. V. Jezak of the University of Minnesota for making available bound state wave functions which were used in checking calculations. Discussions with Dr. R. M. Eisberg and A. J. Krominga of the University of Minnesota and Dr. M. A. Melkanoff, Dr. F. A. Moszkowski, and Dr. D. L. Pursey of UCLA have been very productive. We are indebted to Dr. J. S. Nodvik of the University of Southern California for advice concerning certain aspects of the calculations involving spin-orbit splitting.